"The Fourth International Symposium on Computational Wind Engineering CWE2006",

Yokohama, Japan, July 16-19 2006

Exploring the flow around a generic high-speed train under the influence of side winds using LES

Hassan Hemida and Siniša Krajnović
Division of Fluid Dynamics, Department of Applied Mechanics,
Chalmers University of Technology, Gothenburg, Sweden

Abstract

Large-eddy simulation (LES) is made of the flow around a generic train model at two different yaw angles of 90^o and 35^o. The Reynolds number, based on the freestream velocity and the height of the train, is 3×10^5 and 3.7×10^5 for the yaw angles of 90^o and 35^o, respectively. Both the time-averaged and instantaneous flows are explored. The LES results show that the influence of the three-dimensional flow from the nose of the train on the time-averaged wake flow at the 90^o yaw angle is limited to a region of a length of 3.5 train heights from the tip of the nose in the direction of the length of the train. The instantaneous flow shows an unsteady vortex shedding due to the shear layer instabilities on the periphery of the recirculation region and the exterior flow. Weak vortex shedding is found in the case of the 35^o yaw angle. Instead, unstable vortices are found in the wake flow. These vortices detach from and reattach to the train surface in a regular fashion leaving disturbances on the train surface and hence affecting the aerodynamic coefficients.

Keywords: Side wind, LES, train aerodynamics, wake structures.

1 Introduction

Existing knowledge about side wind influences on high-speed trains comes mainly from experimental studies such as those described in [1–4]. The data obtained from the experimental studies are not sufficient to give a full picture of the flow around trains since they are limited to a confined region of a line or plane. Numerical studies such as [5–7] are rare. Most of these studies are based on solutions of the Reynolds Averaged Navier-Stokes (RANS) equations, which describe the time-averaged flow. Chiu & Squire [4] experimentally studied the side wind flow around a generic train model at large yaw angles. They found that the flow changes from that associated to a slender body flow at low yaw angles to an unsteady shedding at yaw angles higher than 40^o. However, the transition mechanism between the two flows was not explained. In this paper, large-eddy simulation with a standard sub-grid Smagorinsky model with model constant $Cs = 0.1$

is made for the flow around a generic high-speed train under the influence of side wind at two yaw angles: 90^o and 35^o. The Reynolds number, based on the freestream velocity and the height of the train, is 3×10^5 and 3.7×10^5 for yaw angles 90^o and 35^o , respectively. Finite volume in-house code is employed to solve the governing turbulent equations using parallel computations in complex multi-block domains. Both the time-averaged and instantaneous flows are investigated. The LES results for the 90^o yaw angle are validated using the experimental data of Chiu & Squire [4] while the LES results of the 35^o yaw angle are compared with the experimental data of Copley [3].

2 Computational model and boundary conditions

The train model used in this paper is the one of Copley [3]. This model is chosen due to its simplicity and the existence of experimental data. It consists of two parts: train body and nose (more details about the simplified model are found in [3]). The computational domain is shown in Figure 1. The inlet plane is kept parallel to the train axis to ensure constant boundary layer thickness approaching the train surface. Two computations with different numbers of nodes are made for each yaw angle. The fine meshes contain 11 and 14 million nodes and the coarse meshes contain 8 and 6 million nodes for the 90^o and 35^o yaw angles, respectively. The flow enters the channel with uniform velocity constant in time. No-slip boundary conditions are used on the train body and floor. Wall functions are used on the lateral walls and roof. Convective boundary conditions are used at the channel exit. Homogeneous Neumann boundary conditions are used for the pressure at all boundaries.

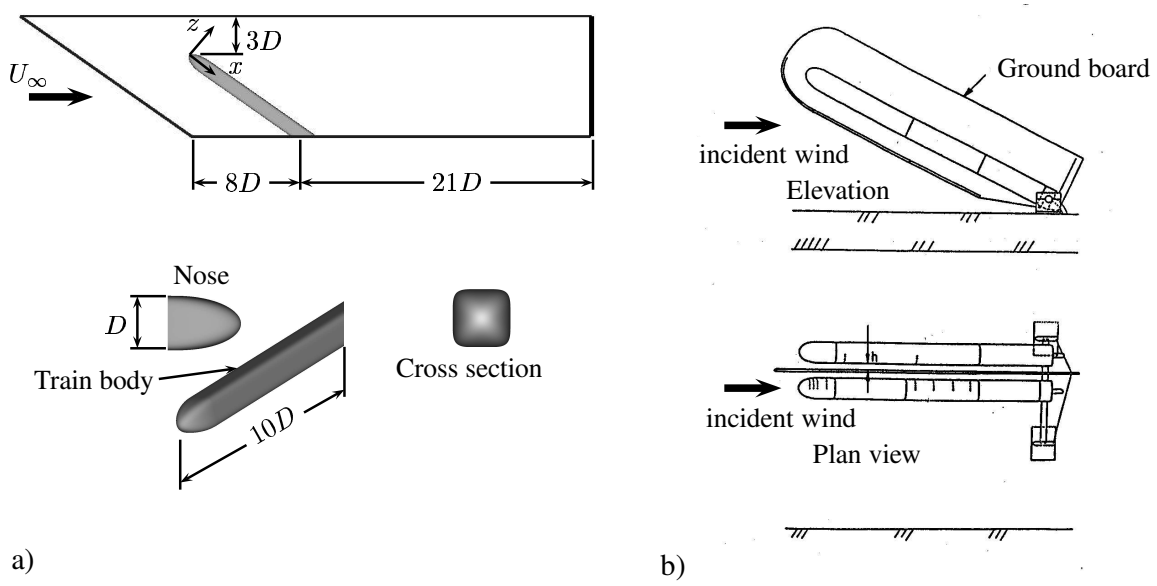

Figure 1: Computational domain and simplified model. (b) Experimental set-up for the 35^o yaw angle.

3 Results

The time-averaged data are collected using 100,000 time steps. This corresponds to a total simulation time of 10 sec ($t^* = tU_\infty/D = 80$). These data are used to explore the time-averaged flow around train models. The LES time-averaged surface pressure distribution is compared with the experimental data in Figure 2. Good agreement is obtained between LES results and the experiment in the case of the 90^o yaw angle. Figure 1b shows the experimental set-up used for the 35^o yaw angle, which is different from our set-up. In the experiment, two models are used (one is a mirror model to the other one used for measurements) to simulate the relative motion of the train with respect to the ground. In addition, a trip wire is used to suppress the separation on the roof-side face. Figure 2b shows that the LES results for the 35^o yaw angle suffer from these differences in the set-ups. The LES underestimates the pressure under the body due to the difference between the LES and the experimental set-ups. LES shows an overestimated pressure on the roof-side face due to the flow separation. Good agreement is obtained on the other faces of the model. Figure 2 shows also the results from the coarse mesh simulations.

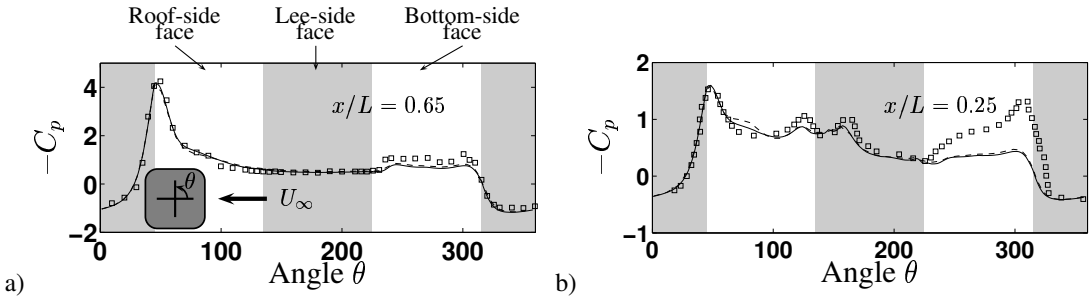

Figure 2: Local pressure coefficient. (a) 90^o yaw angle. (b) 35^o yaw angle. LES using fine mesh (solid line); LES using coarse mesh (dashed line); experimental data (symbols).

Figure 3 shows the time-averaged flow structures around the model in the case of the 35^o yaw angle by means of streamlines projected on the vortex cores. The flow around the nose rolls up to form two vortices, V_{c1} and V_{c2}, as shown in Figure 3. Vortex V_{c1} stretches in the direction of the length of the train. It grows in size but remains attached to the train surface. On the other hand, vortex V_{c2} detaches from the surface shortly after its onset. A number of weak vortices, V_{cr}, are born on the lee-side upper edge of the train. They roll up and merge with the strong vortex, V_{c1}. The underbody flow forms several vortices, V_{c3}, V_{c4} and V_{c5}, at the lee-side bottom edge. These vortices are detached from the surface and convected downstream in the wake flow. Figure 4 shows the development of the major vortices in the time-averaged flow by means of streamlines and velocity vectors projected to a number of plane cross-sections. It shows that the upper wake vortex, V_{c1}, detaches from the lee-side face at $x/L \approx 0.6$. Along the distance where V_{c1} remains attached to the surface, a number of vortices are formed and detach on the lower part of the face. Instantaneous pictures (not shown here) similar to that in Figure 4 show that the center of the upper vortex, V_{c1}, is fixed in space but that its

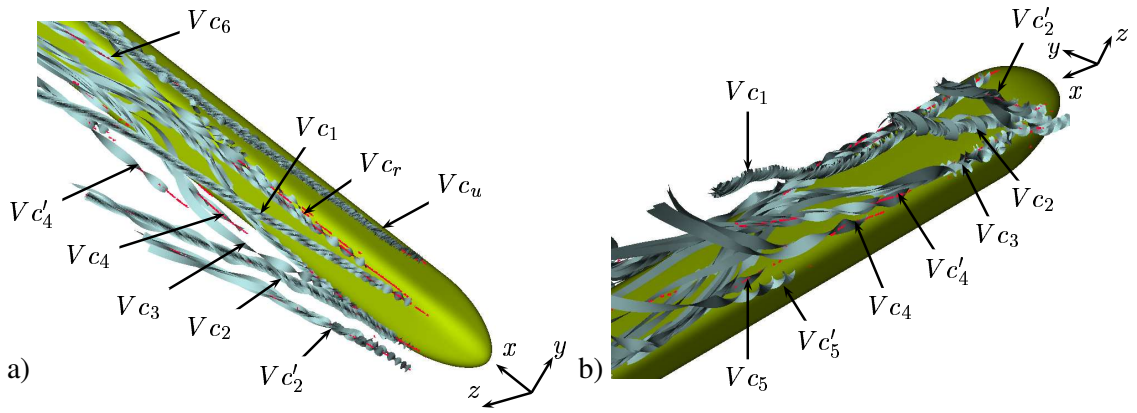

Figure 3: Train at the 35^o yaw angle. Time-averaged flow structures. (a) View from above and the lateral side on the rear of the train. (b) View from below and the lateral side of the rear end of the train.

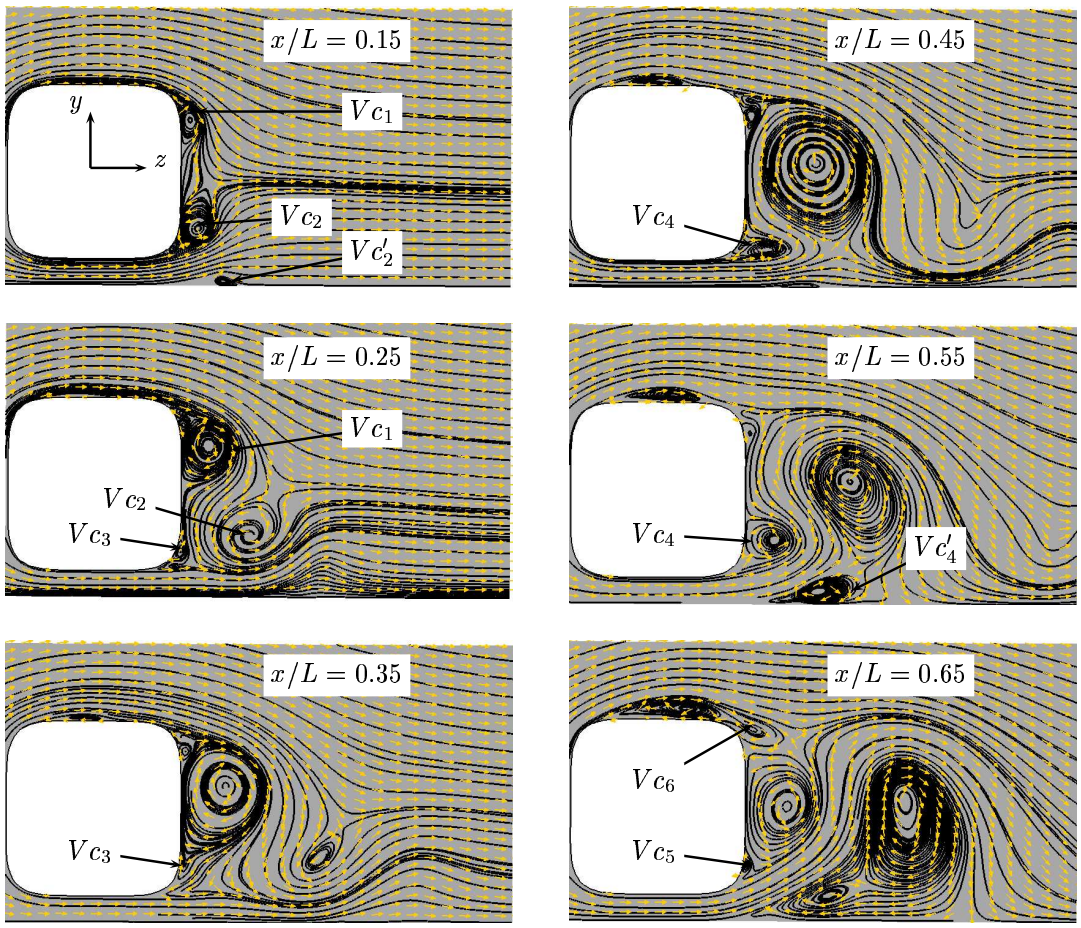

Figure 4: Time-averaged streamlines and velocity vectors projected onto numbers of y-z planes showing the development of the flow structures in the case of the 35^o yaw angle.

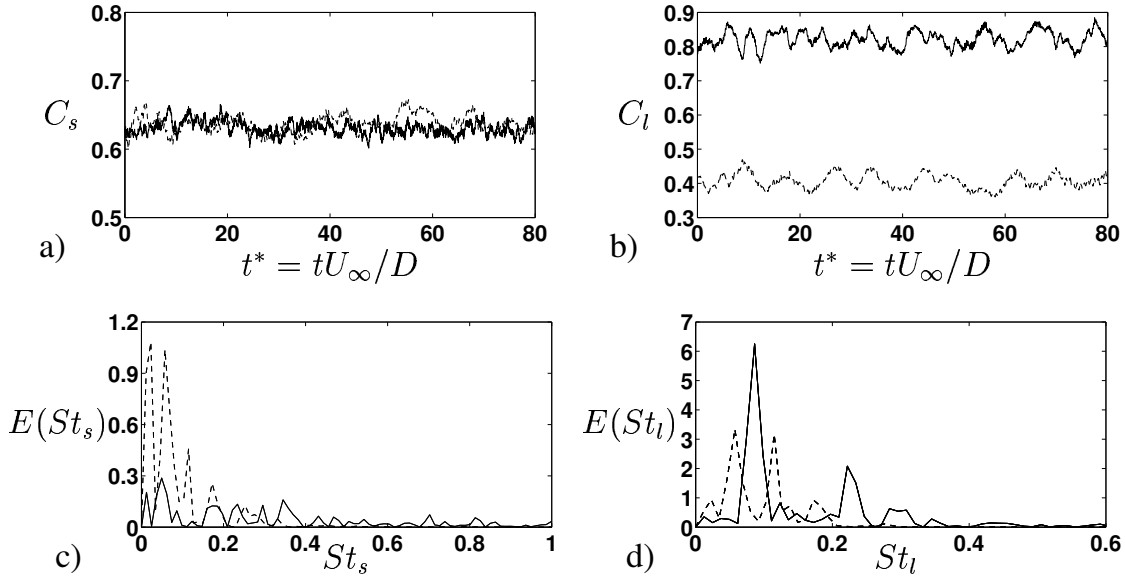

Figure 5: (a) and (b) are the side and lift force coefficients, respectively. (c) and (d) are the autopower spectra of the side and the lift force coefficients, respectively. 90^o yaw angle (solid line); 35^o yaw angle (dashed line)

size changes with time. The lower vortices are not stable and their centers move in a horizontal plane parallel to the ground.

In the case of the 90^o yaw angle, two recirculation bubbles are found in the wake flow. Their centers are parallel to the length of the train after a distance $x/L \approx 0.35$ from the tip of the nose. This flow has strong unsteady vortex shedding, which influences the instantaneous stability of the recirculation bubbles. Snapshots of these bubbles show that their sizes are not constant and their centers are not fixed in space. The instability and movement of the wake vortices at both the 90^o and the 35^o yaw angles disturb the instantaneous train surface pressure. Typical aerodynamic force coefficients are shown in figures 5a, 5b. These figures show that the time-averaged value of the side force coefficient does not change much with the yaw angle. This is due to the high stagnation pressure in the streamwise face next to the side wall and the lower pressure in the lee-side face resulting from the formation of the wake vortices in the case of the 35^o side wind yaw angle. On the other hand, a lower lift coefficient is obtained for the 35^o side wind yaw angle. This is due to the lower pressure that forms on the upper face of the train in the case of the 90^o side wind yaw angle.

To determine the frequencies of the different flow motions, autopower spectra of the time varying signals of the force coefficients are computed. Figures 5c and 5d show these spectra for the side and the lift force coefficients, respectively. The dominating flow frequencies for the 35^o side wind yaw angle are lower than those from the 90^o side wind yaw angle case. These frequency spectra reflect the difference in flow behavior for the large and small side wind yaw angles. In the case of the large yaw angles, the flow is dominated by unsteady vortex shedding with high frequency. In contrast, at low side wind yaw angles, the flow is similar to flow around a slender body, where attachment

and detachment of wake vortices dominate over the unsteady vortex shedding. The frequency of these motions is lower than the shedding frequency.

4 Conclusion

LES was successfully employed to predict the side wind flow around a generic train. The LES results are in a good agreement with experimental investigations. The side wind flow at a 90^o yaw angle is shown to be predominantly unsteady vortex shedding while the side wind flow at lower yaw angles is similar to that around a slender body. At low yaw angles the underbody flow rolls up to shed vortex sheets at successive points along the length of the train. These vortices are highly unsteady. The LES results also show that the recirculation regions are more stable for the 90^o side wind yaw angle.

References

[1] C.J. Baker. Some complex applications of the wind loading chain. *Journal of Wind Engineering and Industrial Aerodynamics*, 91:1791–1811, 2003.

[2] M. Suzuki, K. Tanemoto, and T. Maeda. Aerodynamic characteristics of train/vehicles under cross winds. *Journal of Wind Engineering and Industrial Aerodynamics*, 91:209–218, 2003.

[3] J. M. Copley. The three-dimensional flow around railway trains. *Journal of Wind Engineering and Industrial Aerodynamics*, 26:21–52, 1987.

[4] T. W. Chiu and L. C. Squire. An experimental study of the flow over a train in a crosswind at large yaw angles up to 90^o. *Journal of Wind Engineering and Industrial Aerodynamics*, 45:47–74, 1992.

[5] B. Diedrichs. On computational fluid dynamics modelling of crosswind effects for high-speed rolling stock. *IMechE*, 217(F):203–226, 2003.

[6] F. Durst W. Khier, M. Breuer. Flow structure around trains under side wind conditions: a numerical study. *Computers & Fluids*, 29:179–195, 2000.

[7] H. Hemida, S. Krajnović, and L. Davidson. Large-eddy simulations of the flow around a simplified high speed train under the influence of a cross-wind. In *17th AIAA Computational Fluid Dynamics Conference*, Toronto, Ontario, CANADA 6-9 Jun, 2005.